Available online at www.sciencedirect.com
SCIENCE DIRECT®
Journal of Sound and Vibration 286 (2005) 123–144
JOURNAL OF SOUND AND VIBRATION
www.elsevier.com/locate/jsvi

The damping performance of a single particle impact damper

M.R. Duncan, C.R. Wassgren*, C.M. Krousgrill

School of Mechanical Engineering, Purdue University, 1288 Mechanical Engineering, 585 Purdue Mall, West Lafayette, IN 47907-2088, USA

Received 22 September 2003; received in revised form 16 July 2004; accepted 30 September 2004
Available online 24 December 2004

Abstract

This paper presents results from computer simulations used to investigate the damping performance of a single particle vertical impact damper over a wide range of excitation frequencies and amplitudes, particle-to-structure mass ratios, lid clearance ratios, structural damping ratios, and coefficients of restitution. Measurements of the damping performance, particle flight times, and structure contact times are presented. Performance at both the structure's undamped natural frequency and off-resonant conditions are studied in depth. Maximum damping at a fixed oscillation frequency occurs at an optimal lid height that increases with increasing mass ratio, increasing structural damping ratio, but decreases with coefficient of restitution. The corresponding maximum degree of damping increases with increasing mass ratio and coefficient of restitution, but decreases with increasing structural damping ratio. Field plots of the damping ratio are also presented as functions of oscillation amplitude and frequency to demonstrate the damper performance over a range of design parameters and operating conditions.

1. Introduction

A single particle impact damper is a common vibration-damping device consisting of a single particle enclosed within a container. The container can either be mounted directly to the structure to be damped or can be designed as an integral part of the structure, often as holes drilled directly

*Corresponding author. Tel.: +1 765 494 5656; fax: +1 765 494 0539.
E-mail address: wassgren@purdue.edu (C.R. Wassgren).

0022-460X/$ - see front matter © 2004 Elsevier Ltd. All rights reserved.
doi:10.1016/j.jsv.2004.09.028

Nomenclature

[]	The square brackets in the following list indicate the quantity's dimensions with M, L, T, and F representing mass, length, time, and force, respectively.
a	base vibration amplitude [L]
c'	damping ratio of the primary system without the impact damper $c' = c/(2\sqrt{km_S})$ [dimensionless]
c	viscous damping coefficient [M/T]
d	damping performance of the impact damper $\sigma_{\text{undamped}}/\sigma_{\text{damped}}$ [dimensionless]
d_f	ratio of the system's kinetic energy converted into heat during an oscillation cycle to the maximum kinetic energy of the structure during the cycle, defined by Friend and Kinra [11] [dimensionless]
f_0	force applied to the primary system [F]
g	gravitational acceleration [L/T^2]
h	clearance of the particle [L]
h'	dimensionless clearance ratio: $h' = h\omega_N^2/g$ [dimensionless]
k	spring stiffness [F/L]
m_P	mass of the particle [M]
m_S	mass of primary structure [M]
m'	dimensionless mass ratio: $m' = m_P/m_S$ [dimensionless]
$\dot{y}_P$	velocity of the particle [L/T]
$\dot{y}_S$	velocity of the structure [L/T]
$\dot{y}_{\max}$	maximum velocity of the structure [L/T]
a'	dimensionless base amplitude: $a' = a\omega_N^2/g$ [dimensionless]
ε	coefficient of restitution for particle–structure impacts [dimensionless]
σ_{undamped}	standard deviation of the structure's position without an impact damper [L]
σ_{damped}	standard deviation of the structure's position with the impact damper [L]
ω'	dimensionless frequency ratio: $\omega' = \omega/\omega_N$ [dimensionless]
ω	radian frequency of excitation [1/T]
ω_N	natural [radian] frequency of the primary system [1/T]
ϕ	phase angle in radian of the force applied to the primary system [dimensionless]

into the structure [1,2]. Damping is achieved by modifying the structure dynamics through collisions between the particle and the container walls and by dissipating energy through inelastic impacts [3].

The advantages to using impact dampers over traditional damping devices are that impact dampers are inexpensive, simple designs that provide effective damping performance over a range of accelerations and frequencies [4–6]. In addition, impact dampers are robust and can operate in environments that are too harsh for other traditional damping methods [7]. Vibration damping with impact dampers has been used in a wide variety of applications including vibration attenuation of cutting tools [8], television aerials [9], turbine blades [10,11], structures [12], and plates, tubing, and shafts [1,13–15].

Despite their simple design, the dynamics of impact dampers can be very complex. The particle and container trajectories are continuous, but not smooth due to impacts. The trajectories may also exhibit multiple stable solutions [8,17,18] and fixed point, periodic orbits and local bifurcations [19] for particular combinations of the system parameters. Factors affecting the damper dynamics include the amplitude and frequency of the forcing vibrations, the masses of the particle and structure, the structural stiffness and damping, the dimensions of the impact damper container, the coefficient of restitution of the impacts, and the acceleration due to gravity. Indeed, there has been little research on how impact dampers perform over a wide range of these parameters.

Previous analytical studies of impact dampers have focused on periodic particle and container trajectories. Popplewell et al. [20] found that impact dampers are most effective when two equi-spaced collisions (one with the container floor and one with the container lid) occur during each oscillation cycle, a condition that occurs only for specific parameters [21]. In addition to periodic trajectories, most of these previous studies have focused on horizontal dampers, i.e. the damper is oriented such that gravitational acceleration is not a factor. Sadek and Mills [16] found that gravity diminishes the effectiveness of an impact damper since the collisions are no longer equi-spaced and the momentum impulses delivered during lid and floor impacts are not equal.

Several investigators [4–6,21] have used their analyses to produce design charts presenting the damping performance for a horizontal impact damper as a function the system parameters such as the particle-to-structure mass ratio, structural damping ratio (without the impact damper), lid clearance ratio, and coefficient of restitution. Most of these charts are specifically for a system operating at the structure's natural frequency with two symmetric impacts per cycle and only a few charts include variations in the forcing amplitude despite an impact damper's inherent dependence on this parameter. These previous studies indicate that an impact damper is more effective as the structural damping ratio decreases and the particle-to-structure mass ratio increases. In addition, these previous studies have shown that damping is maximized at a critical clearance ratio. There are some discrepancies, however, as to how coefficient of restitution affects damping performance. Dokainish and Elmaraghy [5] and Popplewell and Liao [6] indicate that increasing the coefficient of restitution increases damping performance while Pinotti and Sadek [21] state the opposite trend. Dokainish and Elmaraghy further indicate that decreasing the mass ratio reduces the sensitivity to the coefficient of restitution. Bapat and Sankar [4] found both analytically and experimentally that maximum damping performance for a freely decaying system occurred at a coefficient of restitution of 0.3. The reason for these discrepancies remains unclear although it should be noted that each of these studies investigated different vibration amplitudes.

Several researchers have also investigated the performance of impact dampers experimentally [4,21–23]. In general, these experimental studies have corroborated analytical predictions. These studies have also investigated, to a limited degree, the response of an impact-damped system over a range of forcing frequencies and amplitudes. Ema and Marui [22] found that for the free response decay of a spring mass system, the damping rate of the system increases with increasing vibration amplitude with the best damping performance occurring for particular combinations of the mass and clearance ratios depending on the initial spring displacement. Popplewell et al. [20] found in their forced vibration experiments that excitation frequencies at or slightly above the structure's natural frequency produced positive damping, while frequencies lower than the natural frequency produced negative damping, i.e. the structure vibrates more than without the impact damper. Semercigil et al. [23] performed experiments on impact dampers in combination with tuned mass dampers. The free decay of the response of a system with a tuned mass damper was shown to be reduced by 80% by placing an impact damper inside of the tuned mass damper. The impact damper was shown to be effective for a range of tuning frequencies and relatively unaffected by excitation levels.

A number of investigators have also studied the performance of multi-particle [3,11,24,25] and bean bag impact dampers [26,27–29]. Both multi-particle and bean bag dampers utilize many particles within the damper container with multi-particle dampers having freely moving particles and bean bag dampers typically constraining the particles within a flexible bag. In

general, multi-particle and bean bag dampers produce less shock and noise and are less sensitive to the vibration parameters, gravity, and container clearance dimensions than their single particle counterparts [11]. The performance of multi-particle dampers, however, is affected by the size of the particles used within the damper with smaller particles producing greater damping performance at larger amplitudes [11]. Experiments have shown that multi-particle systems can be modeled with reasonable accuracy as single particle dampers [24]. Experiments have also shown that bean bag dampers can produce more effective damping than single particle impact dampers [29].

While these previous studies have provided valuable insight into the dynamics of impact dampers and how to optimize their design, there still remains a lack of information on how impact dampers perform when operating over a wide range of conditions. For example, few studies have examined excitation frequencies away from resonance or have looked at the effects of excitation amplitude. Popplewell et al. [20] and Bapat and Sankar [4] have shown, in limited studies, that the optimal impact damper parameters can vary at off-resonant conditions. This paper presents results from computer simulations that are used to investigate the damping performance of vertical impact dampers over a wide range of oscillation frequencies and excitation amplitudes, particle-to-structure mass ratios, lid clearance ratios, coefficients of restitution, and structural damping ratios. Additional investigations of the system dynamics are presented for significant operating conditions such as where peaks in the damping performance are observed and where the performance is sensitive to small changes in operating conditions.

2. Computational model

A computer simulation was developed in order to investigate the performance of an impact damper over a wide range of conditions. The modeled system consists of a base oscillating sinusoidally with amplitude, a, and radian frequency, ω. A rigid structure is attached to the base with a damped spring of stiffness, k, and damping, c. Mounted to the structure is a container of height, h, where m_s is the combined mass of the structure and container. Within the container is a particle with negligible diameter and mass, m_P. Impacts between the container and particle are characterized by a coefficient of restitution, ε. The structure and impact damper are subject to gravitational acceleration, g. A schematic of the system is shown in Fig. 1.

The structure's acceleration between impacts, $\ddot{y}_S$ (the overdots indicate differentiation with respect to time) is given by

$$\ddot{y}_S = -\frac{k}{m}(y_S - y_b) - \frac{c}{m}(\dot{y}_S - \dot{y}_b) - g, \tag{1}$$

where $m = m_S$ when the particle is in flight and $m = m_S + m_P$ when the particle remains in contact with the container floor or lid for an extended period (when the coefficient of restitution is zero, for example).

The base acceleration, $\ddot{y}_b$, is prescribed to be

$$\ddot{y}_b = -a\omega^2 \sin(\omega t). \tag{2}$$

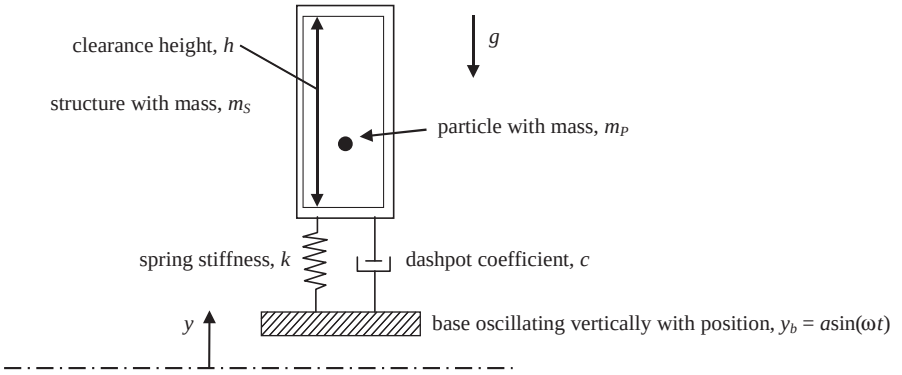

Fig. 1. A schematic of the modeled vertical impact damper system.

Note that in the models of Dokainish and Elmaraghy [5] and Popplewell and Liao [6] a sinusoidal force is imposed directly to a damper with a fixed base as opposed to prescribing the base motion. Correlation between the two approaches is achieved by noting that the amplitude of the applied force, f_0, and phase angle ϕ, can be written as

$$f_0 = a\sqrt{k^2 + c^2\omega^2}, \tag{3}$$

$$\tan(\phi) = \frac{c\omega}{k}. \tag{4}$$

The particle's acceleration is equal to the structure's acceleration when the particle is in contact with the container for extended periods. However, when the particle is in contact with the container floor and $\ddot{y}_S < -g$, or when the particle is in contact with the container lid and $\ddot{y}_S > -g$, then the particle loses contact with the container and has an acceleration equal to that of gravity:

$$\ddot{y}_P = -g. \tag{5}$$

Impacts between the particle and the container are modeled using conservation of linear momentum and a coefficient of restitution, ε. Conservation of linear momentum gives

$$m_S\dot{y}_S^+ + m_P\dot{y}_P^+ = m_S\dot{y}_S^- + m_P\dot{y}_P^-, \tag{6}$$

where the superscripts "+" and "−" indicate conditions just after and prior to the impact, respectively. The coefficient of restitution for the impact, ε ($0 \leqslant \varepsilon \leqslant 1$) is defined as the negative of the ratio of the relative velocity between the structure and particle after impact to the relative velocity before impact:

$$\varepsilon = -\left(\frac{\dot{y}_S^+ - \dot{y}_P^+}{\dot{y}_S^- - \dot{y}_P^-}\right). \tag{7}$$

Note that for real impacts the coefficient of restitution is a function of the impact velocity [30] with the coefficient of restitution decreasing with the impact velocity raised to the $-1/5$ power [31]. This velocity dependence is not considered in the present model nor has it been considered in

most previous analytical and computational studies. Popplewell and Semercigil [29] did, in effect, include a velocity-dependent coefficient of restitution in their studies of bean bag dampers and found that such a model did slightly improve predictions of the transient and steady-state response of the structure.

The simulation integrates the particle and structure equations of motion (the container is mounted directly to the structure) in time using an Euler integration scheme with a simulation time step of $\Delta t = 1.0 \times 10^{-5}$s. Test simulations were run with smaller time steps to verify that the results are insensitive to further decreases in time step.

The simulation starts the parametric studies with the particle located on the container floor at the static equilibrium position with the initial velocity of the base, i.e.

$$y_S(t=0) = y_P(t=0) = \frac{-(m_S + m_P)g}{k}, \quad y_b(t=0) = 0,$$
$$\dot{y}_S(t=0) = \dot{y}_P(t=0) = \dot{y}_b(t=0) = a\omega. \tag{8}$$

At the end of a simulation, the frequency is incremented and the final particle and structure states are used as the initial conditions for the following simulation. The process repeats over a range of base frequencies and amplitudes.

To make the simulation results more general, the governing equations are written in dimensionless form. The six resulting dimensionless parameters affecting the system dynamics are: base acceleration amplitude, $a' = a\omega_N^2/g$, base frequency, $\omega' = \omega/\omega_N$, structural damping ratio, $c' = c/(2\sqrt{km_S})$, mass ratio, $m' = m_P/m_S$, lid height, $h' = h\omega_N^2/g$, and coefficient of restitution, ε. The structure's undamped natural frequency (without the impact damper) is $\omega_N = \sqrt{k/m_s}$. Note that the baseline coefficient of restitution has a value of zero. This value was chosen so that the results from this study can be extended to multiple-particle and bean bag dampers where the effective coefficient of restitution is approximately zero [26]. The effects of non-zero coefficients of restitution are presented later.

Several simulations using different dimensional parameters, but identical dimensionless values, were run to verify that the given dimensionless parameters produce identical dimensionless system responses. An example is shown in Table 1, where the results varied by less than 0.01%. Note that alternate definitions of the dimensionless lid height have been proposed in the literature. Popplewell and Liao [6] suggest $h/(f_0/k)$ while Pinotti and Sadek [21] and Heiman et al. [32] use h/a and a/h, respectively.

In this work, the effectiveness of the impact damper is quantified by

$$d = \frac{\sigma_{\text{undamped}}}{\sigma_{\text{damped}}}, \tag{9}$$

where σ_{undamped} is the standard deviation of the structure's position without an impact damper and σ_{damped} is the standard deviation of the structure's position with the impact damper. One hundred base oscillations, excluding the initial 25 cycles so that initial transients could be avoided (to be discussed later), were considered for the calculation of σ_{undamped} and σ_{damped}. Values of $d > 1$, $d < 1$, and $d = 1$ indicate positive, negative, and zero effective damping, respectively.

Comparing the standard deviation of the structure's displacement without an impact damper to that with an impact damper allows for the comparison of what the response of the system would be before and after an impact damper is applied. Adding an impact damper changes the system

Table 1
The validity of the selected dimensionless parameters was established by demonstrating that the damping ratio did not change when the dimensional parameters were varied while the dimensionless parameters were held constant. The dimensionless parameters for all four cases given below are, $\omega' = 1$, $a' = 1.0$, $c' = 0.1$, $h' = 0.1$, $m' = 0.1$, and $\varepsilon = 0.3$

Parameters	Case 1	Case 2	Case 3	Case 4
m_S (kg)	1.0	1.5	1.0	1.0
m_P (kg)	0.10	0.15	0.10	0.10
k (N/m)	1000	1000	2000	500
a (m)	0.098	0.015	0.005	0.020
ω (rad/s)	31.63	25.82	44.73	22.36
c (N s/m)	6.3246	7.75	8.95	4.47
h (m)	0.001	0.0015	0.0005	0.002
Damping ratio, d	2.781	2.781	2.781	2.781

resonant peak by adding mass to the system. When looking at results for $\omega' = 1$, increased damping performance is caused by both the change in the system resonant peak and by the impacts from the damper.

The stability of the particle trajectories was studied by randomly varying the initial conditions to observe if different system trajectories appear. Multiple stable solutions were often present, but did not have an appreciable effect on the damping ratio. The stability of impact damper trajectories has been studied in detail in Refs. [17,18,20].

Popplewell and Liao [6] measured damping performance using the ratio of the maximum displacement of the system with the damper to (f_0/k). Dokainish and Elmaraghy [5] used the ratio of the maximum system displacement with the damper to the maximum displacement of the primary system in the absence of the damper. Others, such as Friend and Kinra [3], have used the ratio of system's kinetic energy converted into heat (due to impacts) during an oscillation cycle to the maximum kinetic energy of the structure during the cycle:

$$d_f = \frac{(1-\varepsilon^2)}{\dot{y}^{2-}_{\max}} \left(\frac{m'}{1+m'}\right) \sum_{1}^{i} (\dot{y}^{-}_P - \dot{y}^{-}_S)^2, \tag{10}$$

where i is the number of impacts during an oscillation cycle. The variety of definitions for damping ratio suggests that there is no one "best" way to define the damping performance of an impact damper.

In order to avoid recording data resulting from initial transients, each simulation runs for 25 base oscillation cycles before any data are collected. After this initial period, particle and structure state data are collected for 100 base oscillation cycles. Several additional simulations were run in which the start of the data collection period and the number of data collection cycles were increased. These simulations were performed for the parameters listed in Table 2 at the structure's natural frequency with the dimensionless amplitude varying from 0.1 to 5.0. The damping ratio was found to vary by less than 0.2% for simulations with 100 base oscillation cycles when compared to 1000 base oscillation cycles. These additional simulations demonstrated that the chosen initial transient and data collection periods did not affect the data collected from the simulation.

Table 2
The dimensionless baseline simulation parameters. The structure's undamped natural frequency is $\omega_N = \sqrt{k/m_S}$

Parameter	Baseline value
Mass ratio, $m' = m_P/m_S$	0.05
Damping ratio, $c' = c/(2\sqrt{km_S})$	0.05
Coefficient of restitution, ε	0.0
Lid clearance ratio, $h' = h\omega_N^2/g$	50

3. Results and discussion

First, the impact damper was analyzed for sufficiently small dimensionless base amplitudes, a', where the lid has no effect. Figs. 2a and b show the flight times of the particle, normalized by the base oscillation period, and duration of the time the particle is in contact with the base and lid, also normalized by the base oscillation period, for the baseline simulation parameters (refer to Table 2). Fig. 2c shows the corresponding damping ratio, d. As $a' \to 0$, the structure acceleration remains greater than $-g$ and the particle does not leave the floor, which is indicated by the zero flight time. In this region the impact damper acts to "de-tune" the structure since the structure's natural frequency decreases due to the addition of the particle mass. The damping ratio for the no-flight case is equal to the ratio of the frequency response function for the two cases which reduces to

$$d = \sqrt{\left(\frac{m'}{2c'}\right)^2 + 1}. \tag{11}$$

As the dimensionless base amplitude, a', increases the particle leaves the structure and the normalized flight time approaches a value of one, corresponding to a particle flight time equal to the base oscillation period. Further increases in the dimensionless base amplitude result in a flight time bifurcation with one normalized flight time greater than one, and the other less than one. With further increases in a', the two flight times transition to a single flight time again, but with the system motion repeating every two cycles. An additional bifurcation occurs as the flight times split and transition to motion that repeats every three cycles.

Complex trajectories appear after the particle begins to hit the lid (indicated by the vertical dashed line in Fig. 2). Fig. 2c shows that flight time bifurcations decrease the damping ratio for the no-lid case; however, when the flight time bifurcations occur with lid impacts, the damping ratio increases.

Increasing a' increases the damping ratio until a maximum is reached. Note that over this range of a' the particle hits the lid but does not "stick" since the lid acceleration at impact is greater than $-g$. This can be observed in Figs. 2a and b where the times the particle spends on the floor and lid between successive contacts are plotted.

The maximum damping value occurs when the particle just begins to "stick" to the lid, i.e. the lid acceleration at impact is less than $-g$. Increasing a' further results in decreasing d. Fig. 2b

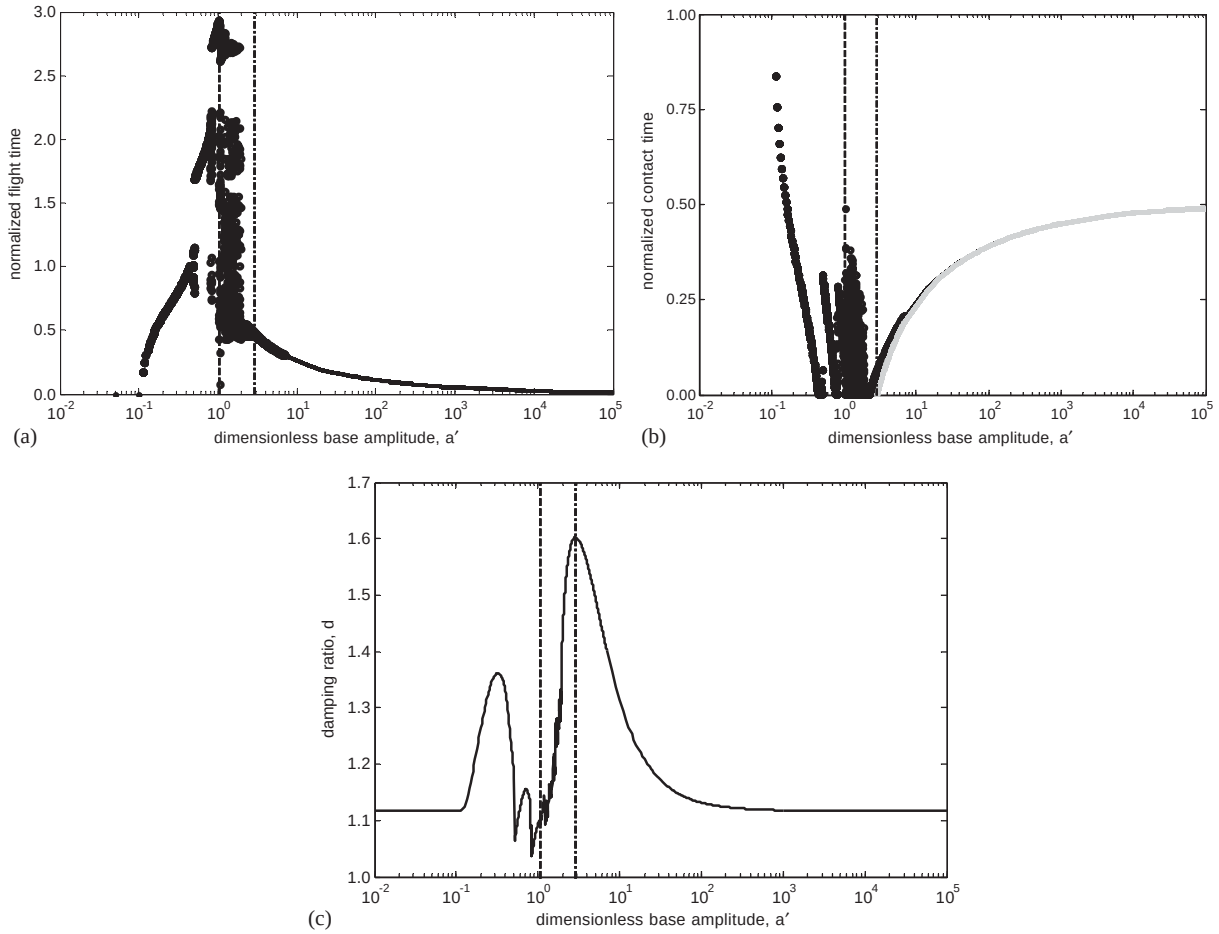

Fig. 2. (a) The particle flight time normalized by the base oscillation period plotted as a function of the dimensionless base amplitude, a', at a dimensionless frequency of $\omega' = 1$. The remainder of the simulation parameters are given in Table 2. (b) The particle contact time with the floor (black) and lid (grey) corresponding to the conditions in (a). (c) The damping ratio, d, corresponding to the conditions in (a). The vertical dashed line indicates when lid impacts start to occur. The vertical dot–dashed line indicates when the particle begins to "stick" to the lid at impact (i.e. $\ddot{y}_S < -g$ at impact). The flight time, corresponds to the time between successive floor/floor, floor/lid, and lid/floor impacts. The floor (or lid) duration corresponds to the time the particle remains on the floor (or lid) after an impact.

shows the flight time of the particle from the base to the lid approaches the flight time from the lid to the base, i.e. the floor/lid collisions become equi-spaced. When the flight times are equal, the effect of gravity becomes negligible and the vertical impact damper behaves essentially as a horizontal impact damper. This transition can be seen in Fig. 2b and will be discussed later when presenting Fig. 5.

As $a' \to \infty$ the particle spends less time in flight and more time in contact with the lid and base. As observed in Figs. 2a and b, the normalized flight time of the particle approaches zero and the contact time with the lid and base approach 0.5. Furthermore, the relative change in the

structure's momentum,

$$\Delta m = \frac{(\dot{y}_S^+ - \dot{y}_S^-)}{\dot{y}_S^+} \frac{\omega}{2\pi}, \tag{12}$$

where the superscripts "+" and "−" indicate conditions just after and prior to the impact, due to a particle impact decreases as indicated in Fig. 3. As a result, the system behaves essentially the same as when $a' \to 0$ and the damping ratio asymptotically approaches its original detuned value.

The effect of the dimensionless lid height on the damping ratio is shown in Fig. 4 where the damping ratio, d, is plotted against the dimensionless base amplitude, a', for a range of dimensionless lid heights, h'. The figure shows that the maximum damping ratio increases with increasing dimensionless lid height, h', to a limiting value as $a' \to \infty$. Note that maximum damping does not appear for $h' \to \infty$ because this occurs at $a' \to \infty$. The a' at which maximum damping occurs increases as the lid height increases.

The damping curves initially follow the $h' \to \infty$ curve, which corresponds to the damping performance of a no-lid container. When the particle makes contact with the lid, the damping curve branches away from this $h' \to \infty$ curve and increases toward the maximum that occurs when the particle just starts to "stick" to the lid (refer to Fig. 2).

The damping ratio data from Fig. 4 are plotted in Fig. 5 as a function of a'/h' (or in dimensional terms, a/h), along with additional h' cases. This plot clearly demonstrates that the damping ratio approaches a limiting value for sufficiently large h'. Furthermore, the damping ratio scales well with a'/h' for sufficiently large lid heights and base amplitudes. The fact that a'/h' collapses the data indicates that gravity is no longer a significant parameter affecting the impact

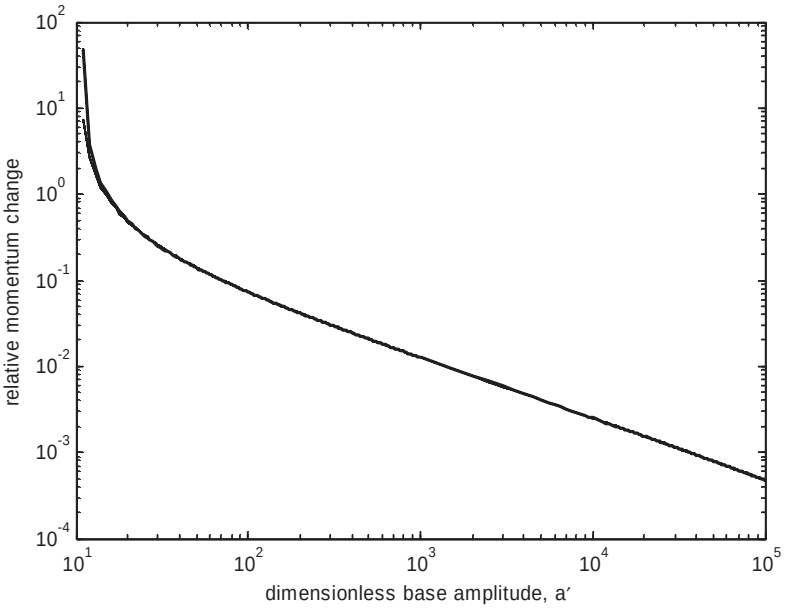

Fig. 3. Relative momentum change of the structure due to particle–floor and particle–lid impacts. The remainder of the simulation parameters are given in Table 2.

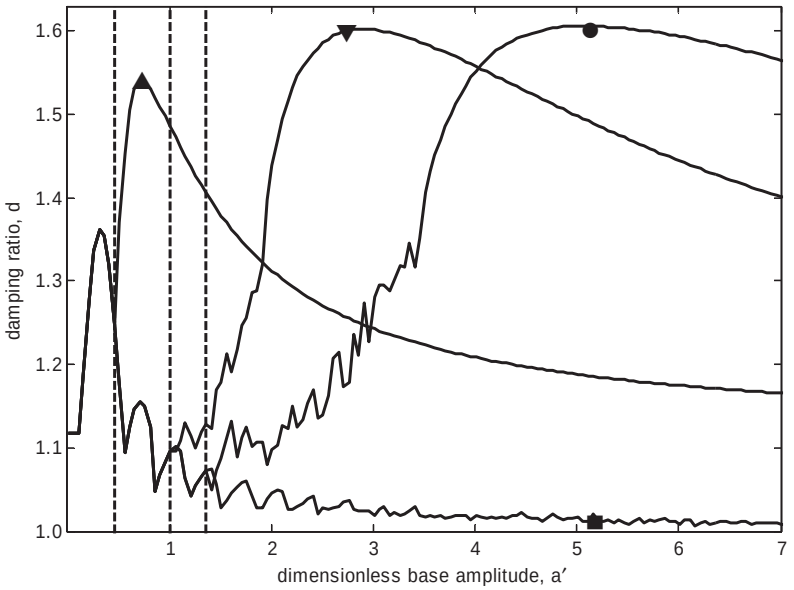

Fig. 4. The damping ratio, d, plotted as a function of the dimensionless base amplitude, a', at a dimensionless frequency of $\omega' = 1$ for a range of dimensionless lid heights, h', where ▲, $h' = 10$; ▼, $h' = 50$; ●, $h' = 90$; ■, $h' = \infty$. The remainder of the simulation parameters are given in Table 2. The vertical dashed lines indicate branch points.

damper's dynamics at large a'/h', i.e. the vertical damper behaves identically to a horizontal damper.

The general trends discussed previously can be summarized in Fig. 6 where a performance plane is plotted using a' values corresponding to the branch points and maximum damping values for varying h'. Below the branch point line the damping performance corresponds to the no-lid solution. Between the branch point and maximum damping line the particle makes contact with the lid, but does not "stick" ($\ddot{y}_S > -g$ at impact). The damping performance increases in this range. Above the maximum damping curve, the particle "sticks" to the lid at impact ($\ddot{y}_S < -g$ at impact) and the damping performance decreases monotonically to its original detuned value.

The dependence of the maximum damping value at the a'/h' value at which this maximum occurs was also investigated as a function of the mass ratio, structural damping ratio, and coefficient of restitution. The maximum damping ratio as a function of the mass ratio, m', is shown in Fig. 7a, and the corresponding optimal a'/h' value is shown in Fig. 7b. Increasing m' increases both the maximum damping value and the optimal a'/h' value in a nearly linear fashion. Similar trends have been reported by Dokainish and Elmaraghy [5], Popplewell and Liao [6], and Pinotti and Sadek [21]. The maximum damping ratio decreases monotonically as the structural damping ratio, c', increases as shown in Fig. 8a, and the corresponding optimal a'/h' ratio increases in an approximately linear fashion as shown in Fig. 8b. Similar results have been presented by Dokainish and Elmaraghy [5]. The maximum damping ratio increases as the coefficient of restitution, ε, increases, with rapidly increasing damping as $\varepsilon \to 1$, as shown in Fig. 9a. However, as will be presented later, the amplitude range over which this increase in

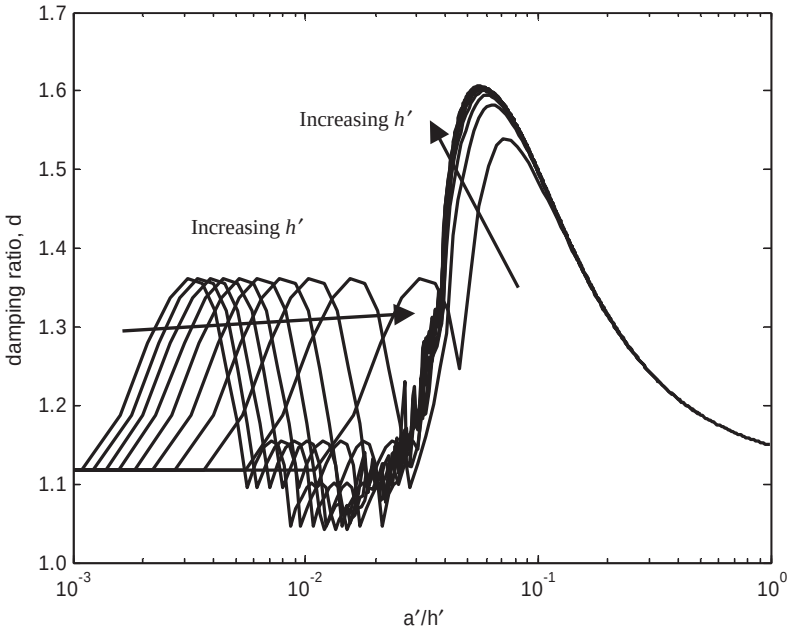

Fig. 5. The damping ratio, d, plotted as a function of the ratio of dimensionless base amplitude to the dimensionless lid height, a'/h', at a dimensionless frequency of $\omega' = 1$ for a range of dimensionless lid heights, h' from 1 to 100. The remainder of the simulation parameters are given in Table 2.

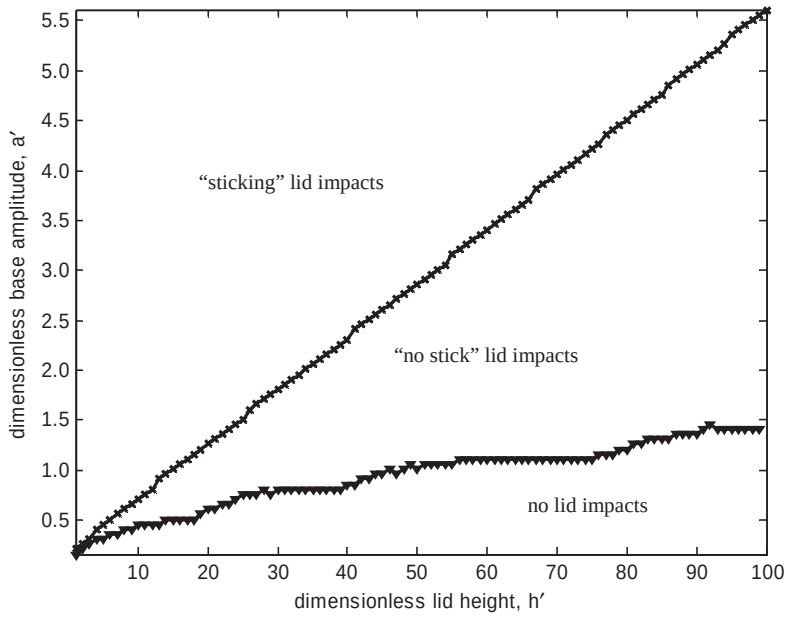

Fig. 6. A performance plane showing maximum damping (*) and branch points (▼) plotted as a function of a' and h'. The remainder of the simulation parameters are given in Table 2.

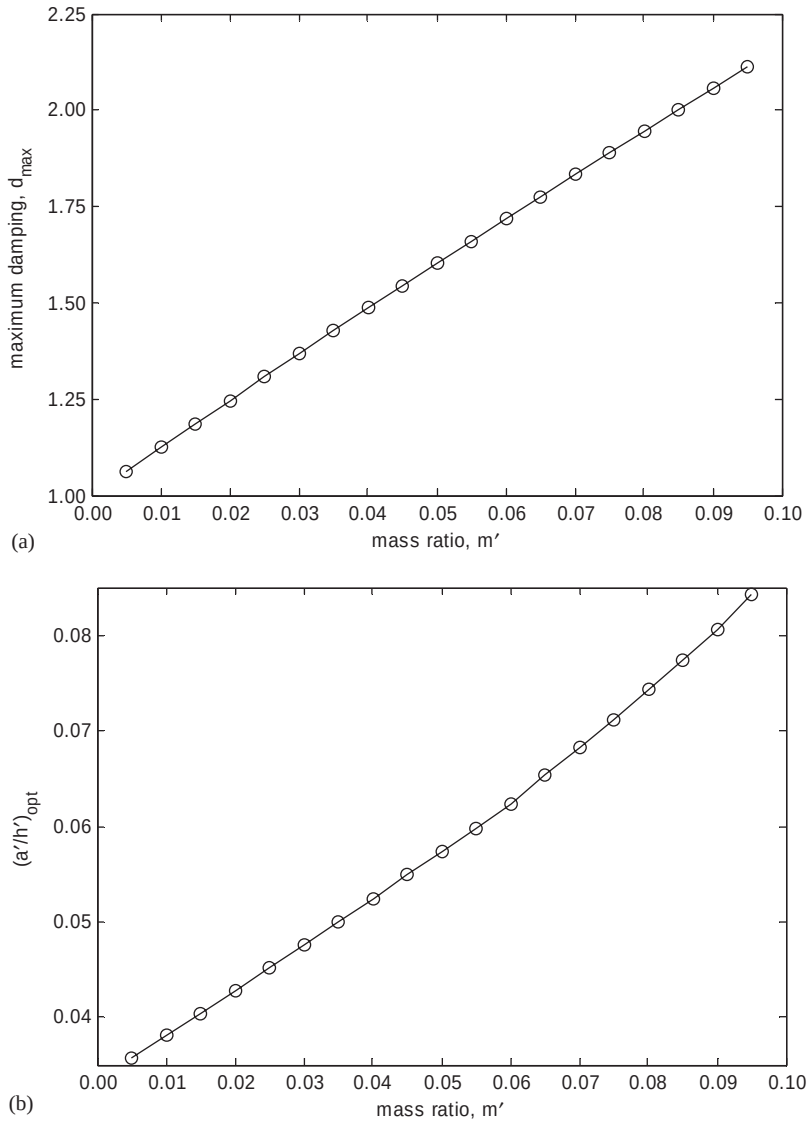

Fig. 7. (a) The maximum damping value, $d_{\max}$, as a function of mass ratio, m', at a dimensionless frequency of $\omega' = 1$. The remainder of the simulation parameters are given in Table 2. (b) The optimal a'/h' ratio at which the maximum damping in (a) occurs.

damping ratio occurs decreases with increasing coefficient of restitution. The optimal a'/h' decreases as ε increases as shown in Fig. 9b. Dokainish and Elmaraghy [5] and Popplewell and Liao [6] have published similar results while Pinotti and Sadek [21] suggest the opposite trends. A possible reason for the discrepancies will be discussed later.

Optimal lid height data from the current simulations are also compared with published design charts [5,6] for validation. The optimal lid heights from simulations using three coefficients of

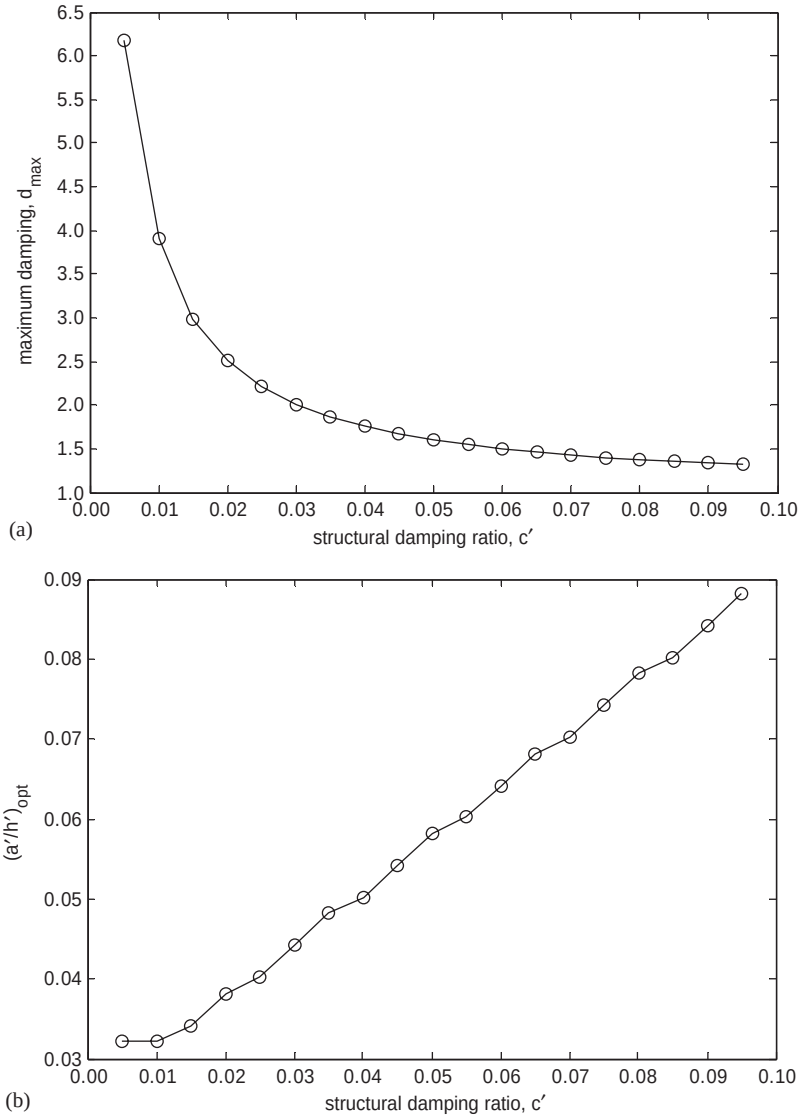

Fig. 8. (a) The maximum damping value, $d_{\max}$, as a function of structural damping ratio, c', at a dimensionless frequency of $\omega' = 1$. The remainder of the simulation parameters are given in Table 2. (b) The optimal a'/h' ratio at which the maximum damping in (a) occurs.

restitution, $\varepsilon = 0.25$, 0.5 and 0.75, vary by less than 2.5% from the data reported in Ref. [6]. The simulations give only a 1.7% difference with the data in Ref. [5] at coefficients of restitution equal to 0.5 and 0.7.

Up to this point all of the results are presented for resonant conditions; however, impact dampers often operate at off-resonant conditions as well. The damping performance at off-resonant conditions was investigated by running simulations over a wide range of forcing

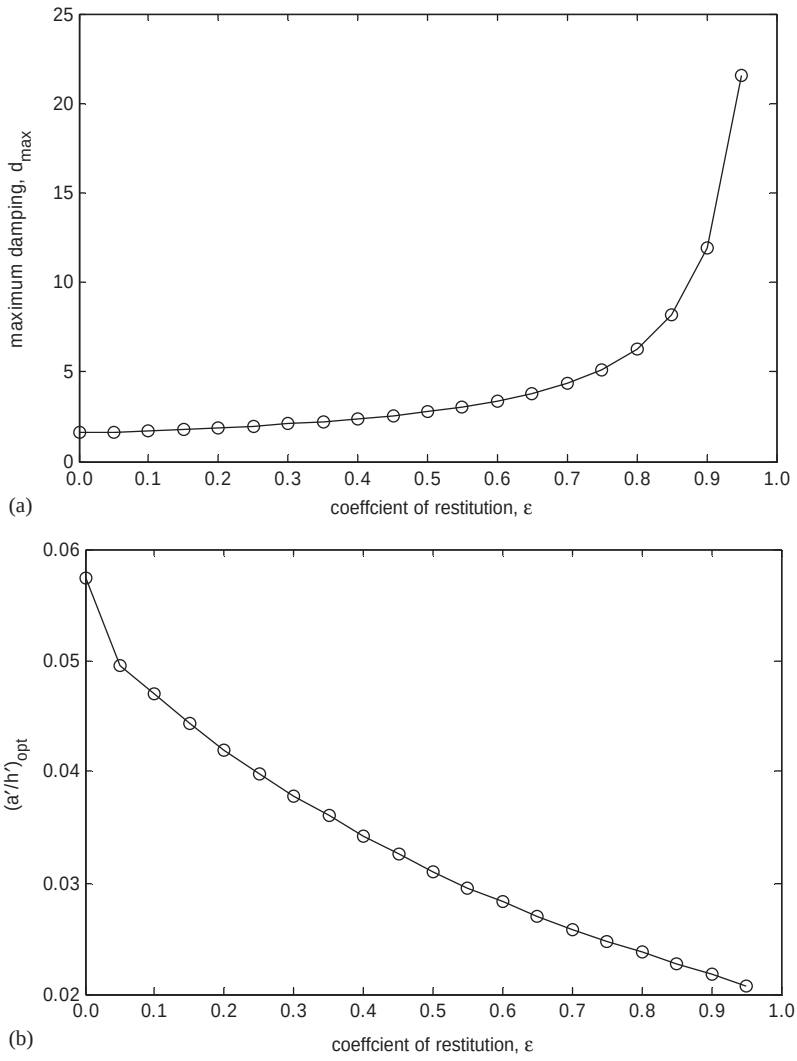

Fig. 9. (a) The maximum damping value, $d_{\max}$, as a function of the coefficient of restitution, ε, at a dimensionless frequency of $\omega' = 1$. The remainder of the simulation parameters are given in Table 2. (b) The optimal a'/h' ratio at which the maximum damping in (a) occurs.

frequencies and amplitudes. The damping results are presented in field plots as functions of the dimensionless mass ratio, m', dimensionless structural damping ratio, c', dimensionless lid height, h', and coefficient of restitution, ε. The simulations utilize the baseline simulation parameters listed in Table 2 unless otherwise noted.

Fig. 10 (a)–(c) show the damping ratio over a range of ω' and a' for mass ratios of $m' = 0.025$, 0.050, and 0.075. Several structures are observed in these figures. The damping ratio, d, has its largest values at base excitation frequencies slightly larger than the structure's natural frequency ($\omega' \geqslant 1$) and for dimensionless base excitation amplitudes greater than a critical value (in this case,

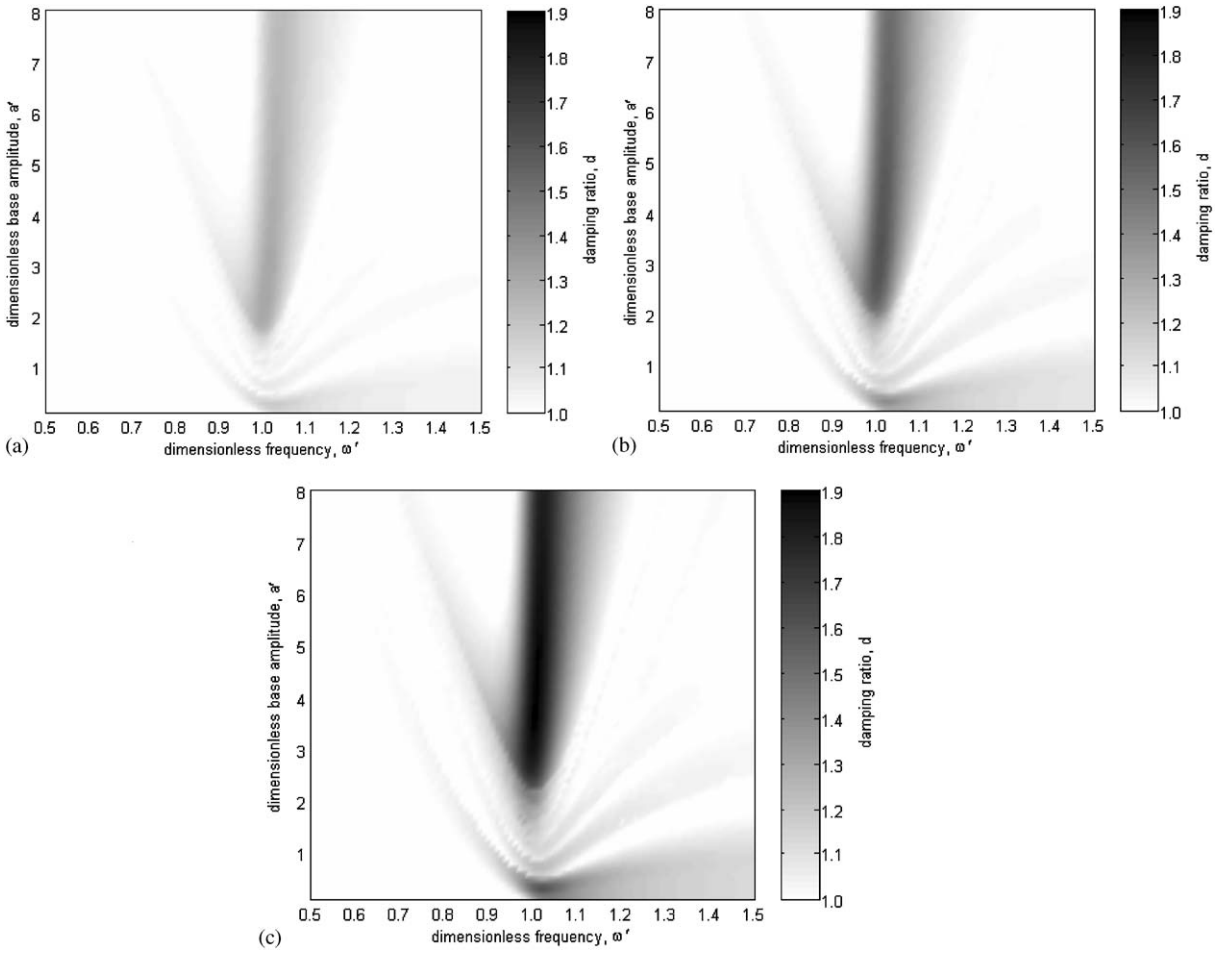

Fig. 10. Field plots of the damping ratio, d, as a function of the dimensionless frequency, ω', and dimensionless base amplitude, a', for mass ratios of (a) $m' = 0.025$, (b) $m' = 0.050$, and (c) $m' = 0.075$. The remainder of the simulation parameters are given in Table 2. Damping ratios less than one are set equal to one for visual clarity.

$a' > 2$). Adjacent to this region, but for $\omega' < 1$, there exists a region of decreased damping. There is a secondary region of large positive damping near $a' < 1$ and $\omega' \geqslant 1$, and again, a region of decreased damping adjacent to it but for $\omega' < 1$. The region of increased damping extends to larger a' values with increasing ω'; however, the damping performance decreases as ω' increases. There are additional regions of positive increased damping with boundaries extending with positive slope ($da'/d\omega' > 0$) for $\omega' > 1$ and negative slope ($da'/d\omega' < 0$) for $\omega' < 1$. These regions become more pronounced with increasing mass ratio and, in some cases, transition abruptly to regions of decreased damping (see, for example, the $m' = 0.075$ case with the branch near $\omega' < 1$ and $a' < 1$). Regions of decreased damping performance exist between these branches. The structures observed in these mass ratio plots also appear in the field plots where the other dimensionless parameters are varied.

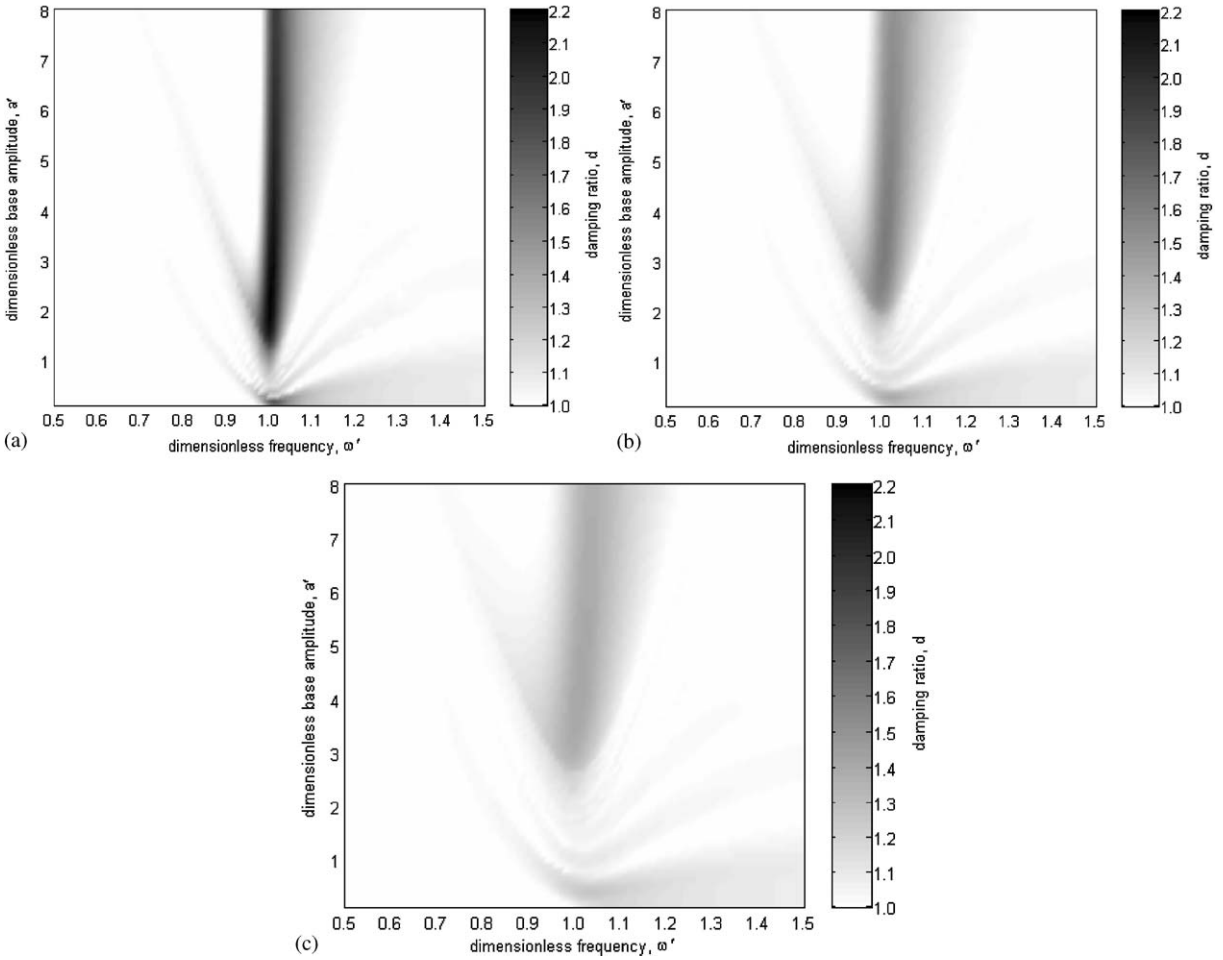

Fig. 11. Field plots of the damping ratio, d, as a function of the dimensionless frequency, ω', and dimensionless base amplitude, a', for structure damping ratios of (a) $c' = 0.025$, (b) $c' = 0.050$, and (c) $c' = 0.075$. The remainder of the simulation parameters are given in Table 2. Damping ratios less than one are set equal to one for visual clarity.

In general, the damping ratio field plots do not have significantly different structure as m' varies; only the magnitudes of the damping ratio appear to vary to any significant degree with the damping ratio increasing with increasing mass ratio. Similar observations have been made by Dokainish and Elmaraghy [5] and Pinotti and Sadek [21].

The effects of the structural damping ratio, c', on the effective damping ratio, d, are shown in Fig. 11 (a)–(c) (corresponding to $c' = 0.025$, 0.050, and 0.075). The trends described previously for varying mass ratio are also observed in these figures. The overall structure of the plots remains similar as c' increases; however, the magnitudes of the damping ratio, d, decrease significantly as c' increases. This dependence on c' is not unexpected since when $c' = 0$, the standard deviation of the structure without the impact damper will approach infinity at $\omega' = 1$ so any amount of damping

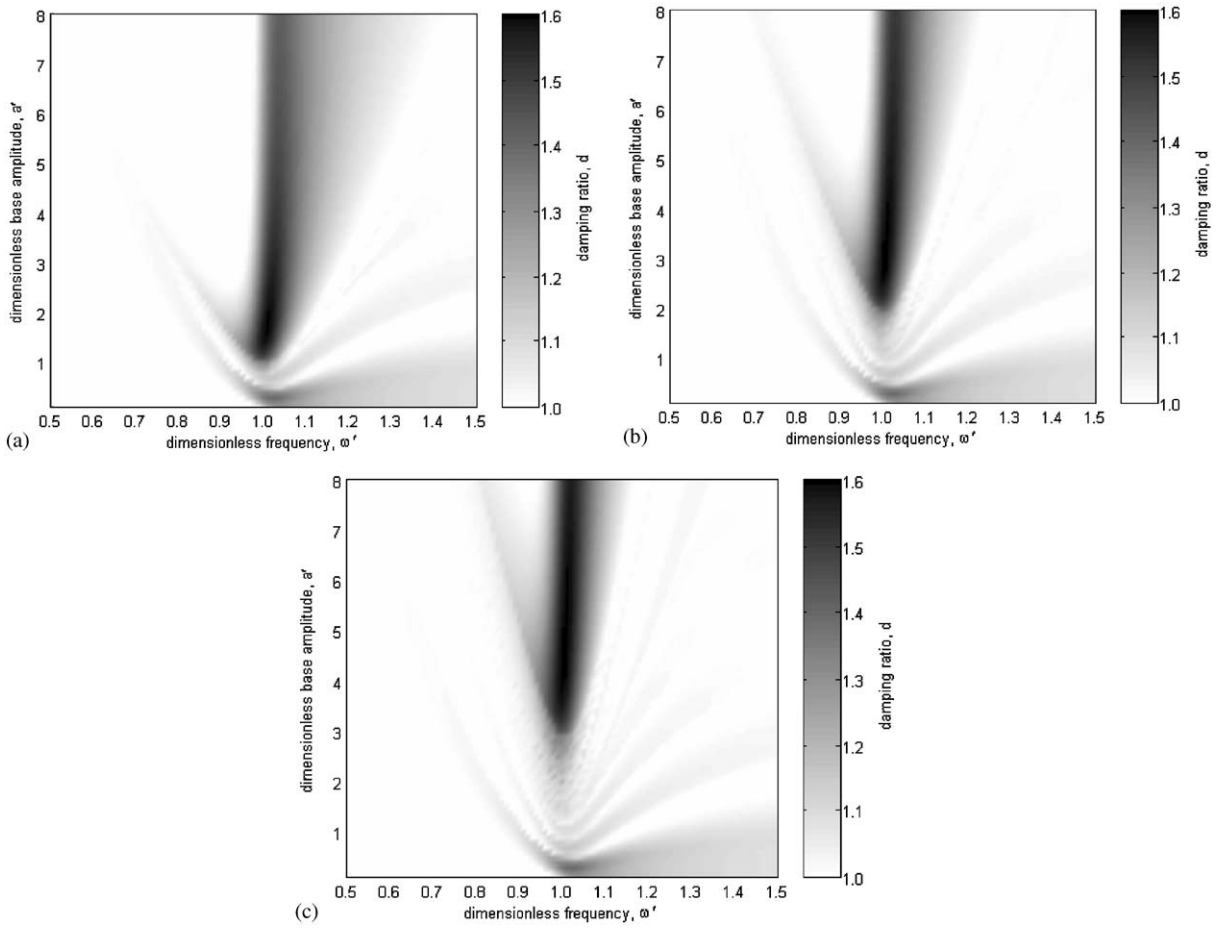

Fig. 12. Field plots of the damping ratio, d, as a function of the dimensionless frequency, ω', and dimensionless amplitude, a', for dimensionless lid heights of (a) $h' = 25$, (b) $h' = 50$, and (c) $h' = 75$. The remainder of the simulation parameters are given in Table 2. Damping ratios less than one are set equal to one for visual clarity.

caused by the impact damper will result in a damping ratio of $d \to \infty$. Dokainish and Elmaraghy [5] have reported similar damping ratio trends with the structural damping ratio.

The effects of the container's lid height, h', on the damping ratio, d, are shown in Figs. 12(a)–(c) (corresponding to $h' = 25$, 50, and 75). As the lid height increases, the a' at which the particle starts to hit the lid increases. For the no-lid impact case, the damping ratios shown in Figs. 12(a)–(c) are identical. Increasing h' stretches the general shape of the damping curve in the a' direction. For sufficiently large values of a', larger than the critical value where the particle just begins to "stick" to the lid, the maximum damping performance is unaffected as observed in Figs. 12(a)–(c) which have the same maximum damping value. Friend and Kinra [3] and Dokainish and Elmaraghy [5] have reported similar damping ratio trends with varying dimensionless lid height.

The effects of the coefficient of restitution of the particle, ε, on the impact damper's damping ratio, d, are shown in Figs. 13 (a)–(d) (corresponding to $\varepsilon = 0.0$, 0.25, 0.50, and 0.75). Increasing

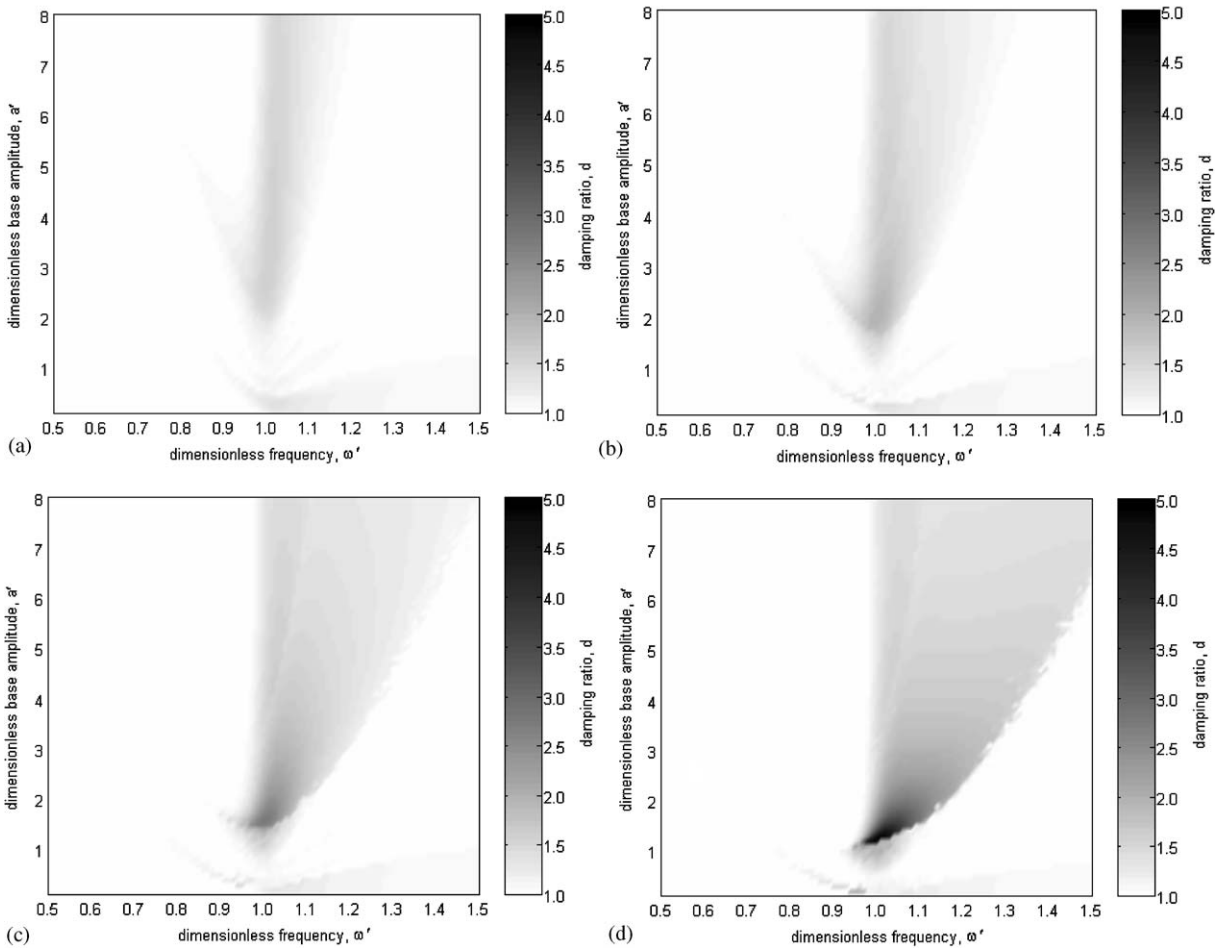

Fig. 13. Field plots of the damping ratio, d, as a function of the dimensionless frequency, ω', and dimensionless base amplitude, a', for coefficients of restitution of (a) $\varepsilon = 0.0$, (b) $\varepsilon = 0.25$, (c) $\varepsilon = 0.50$, and (d) $\varepsilon = 0.75$. The remainder of the simulation parameters are given in Table 2. Damping ratios less than one are set equal to one for visual clarity.

the coefficient of restitution has a significant effect on the overall shape and magnitude of the damping performance field plots. Increasing ε increases both the maximum damping ratio and the frequency range over which the impact damper has increased damping performance. A large region of increased damping occurs for $\omega' > 1$ and broadens with increasing a'. As the maximum damping value increases, a more defined and abrupt transition develops along the lower edge of the branch. These results are similar to those of Popplewell and Liao [6].

Additional useful information is gained by examining the damping ratio behavior at a fixed ω' and varying a' as shown in Fig. 14. Larger values of the coefficient of restitution increase the maximum damping; however, the improved performance occurs over a smaller range of a'. For a' larger than where the maximum damping value occurs, smaller coefficients of restitution provide greater damping. This demonstrates that the performance of the impact damper is not a simple

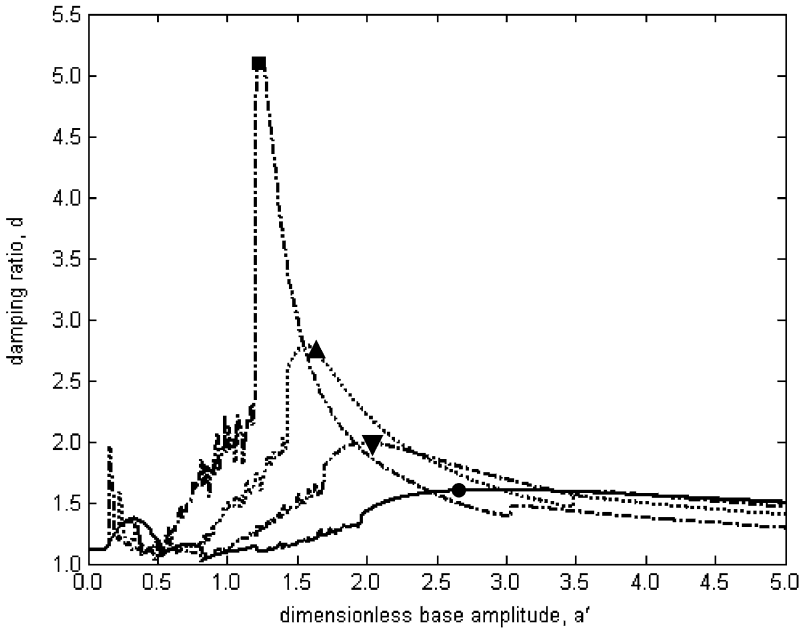

Fig. 14. The damping ratio, d, plotted as a function of the dimensionless base amplitude, a', at a dimensionless frequency of $\omega' = 1$ for varying coefficient of restitution, ε, where ●, $\varepsilon = 0.0$; ▼, $\varepsilon = 0.25$; ▲, $\varepsilon = 0.50$; ■, $\varepsilon = 0.75$. The remainder of the simulation parameters are given in Table 2.

function of the coefficient of restitution, but also depends on whether the value of a' is above or below the value at which maximum damping occurs.

This trend is helpful in explaining the apparent discrepancies reported on how the coefficient of restitution affects the damping performance. Dokainish and Elmaraghy [5] and Popplewell and Liao [6] concluded that increasing the coefficient of restitution increases the damping performance. Fig. 14 shows that this conclusion is valid for assessing the dependence of maximum damping performance on the coefficient of restitution. However, at larger a' the opposite trend is true, an observation made by Pinotti and Sadek [21].

4. Conclusions

The performance of a single particle vertical impact damper was investigated over a range of forcing oscillation amplitudes and frequencies, mass ratios, structural damping ratios, impact damper lid heights, and damper/structure coefficients of restitution. Previous studies have not examined such a large parameter space and instead have focused primarily on conditions at the structure's natural frequency and periodic particle trajectories.

The degree of damping provided by the impact damper at both very small and very large amplitudes approaches the detuned value corresponding to fixing the particle mass directly to the structure. At the structure's undamped natural frequency, maximum damping occurs at an amplitude where the particle just begins to "stick" to the damper lid. Increasing the lid height of

the damper increases the amplitude at which maximum damping occurs, but for sufficiently tall lid heights, has no effect on the degree of damping. In addition, gravity plays less of a role in the damper dynamics at large amplitudes and the vertical damper can be modeled as a horizontal damper.

The lid height at which maximum damping occurs increases with increasing mass ratio and increasing dimensionless structural damping, but decreases with increasing coefficient of restitution. The corresponding maximum damping value increases with increasing mass ratio, increasing coefficient of restitution, and decreasing dimensionless structural damping. These results are generally consistent with those found in previous studies. At oscillation amplitudes greater than the optimal value, damping decreases with increasing coefficient of restitution. This observation may resolve previous conflicting reports [5,6,21] regarding the effect of the coefficient of restitution.

In addition to investigating conditions at the structure's undamped natural frequency, damping investigations were also performed over a range of frequencies. The general structure of these field plots is similar despite variations in mass ratio and dimensionless structural damping ratio. Increasing the dimensionless lid height stretched the general shape of the plot along the dimensionless amplitude axis. At frequencies at and slightly greater than the structure's undamped natural frequency the impact damper provides positive damping for all amplitudes, with the largest damping generally occurring at larger oscillation amplitudes. Negative damping occurs at frequencies slightly less than the structure's undamped natural frequency. Branches of positive and negative damping appear as the forcing frequency diverges from the natural frequency. For sufficiently small amplitudes no lid impacts occur and the degree of damping exhibits local minima and maxima as a result of bifurcations in the particle flight dynamics. The range of amplitudes over which this no-lid-impact region occurs increases with increasing lid height. Of particular note in the field plots is that the frequency range over which positive damping occurs increases with increasing coefficient of restitution. Hence, an impact damper designed to produce the greatest degree of damping should have a large mass ratio, a large coefficient of restitution, and should have a lid height optimized for the expected forcing oscillation amplitude. The large coefficient of restitution will improve the damper's off-resonant performance, but will decrease the performance at off-design oscillation amplitudes.

References

[1] J.R. Fricke, Lodengraf damping-an advanced vibration damping technology, *Sound and Vibration* 34 (7) (2000) 22–27.

[2] C. Tianning, M. Kuanmin, H. Xieqing, M.Y. Wang, Dissipation mechanisms of non-obstructive particle damping using discrete element method, *Proceedings of SPIE International Symposium on Smart Structures and Materials*, 2001, p. 1–8.

[3] R.D. Friend, V.K. Kinra, Particle impact damping, *Journal of Sound and Vibration* 233 (1) (2000) 93–118.

[4] C.N. Bapat, S. Sankar, Single unit impact damper in free and forced vibration, *Journal of Sound and Vibration* 99 (1) (1985) 85–94.

[5] M.A. Dokainish, H. Elmaraghy, Optimum design parameters for impact dampers, *The ASME Publications Design Engineering and Technical Conference* 61 (1973) 1–7.

[6] N. Popplewell, M. Liao, A simple design procedure for optimum impact dampers, *Journal of Sound and Vibration* 146 (3) (1991) 519–526.

[7] E.M. Flint, Experimental measurements of particle damping effectiveness under centrifugal loads, *Proceedings of the Fourth National Turbine Engine High Cycle Fatigue Conference*, 1999, pp. 1–6.
[8] M.M. Sadek, B. Mills, The application of the impact damper to the control of machine tool chatter, *Proceedings of the Seventh International Machine Tool and Die Research Conference*, 1966, pp. 243–257.
[9] H.G. Kaper, The behaviour of a spring mass system provided with a discontinuous dynamic vibration absorber, *Applied Science Research Section A* 5 (10) (1961) 369–383.
[10] K.P. Duffy, R.L. Bagley, O. Mehmed, A self-tuning impact damper for rotating blades, NASA Tech Briefs TSP LEW-168333, 2001, pp. 1–15.
[11] B.L. Fowler, E.M. Flint, S.E. Olson, Design methodology for particle damping, *Proceedings of SPIE Conference on Smart Structures and Materials*, Paper # 4331-20, 2001, pp. 1–12.
[12] S. Chatterjee, A.K. Mallik, A. Ghosh, On impact dampers for non-linear vibrating systems, *Journal of Sound and Vibration* 187 (3) (1995) 403–420.
[13] H.V. Panossian, Structural damping enhancement via non-obstructive particle damping technique, *Journal of Vibration and Acoustics* 114 (1) (1992) 101–105.
[14] E. Skipor, L.J. Bain, Application of impact damping to rotary printing equipment, *ASME Journal of Mechanical Design* 102 (2) (1980) 338–343.
[15] M.D. Thomas, W.A. Knight, M.M. Sadek, The impact damper as a method improving cantilever boring bars, *Journal of Engineering for Industry Transactions of the ASME* 97 (3) (1975) 859–866.
[16] M.M. Sadek, B. Mills, Effect of gravity on the performance of an impact damper: Part 1. Steady-state motion, *Journal of Mechanical Engineering Science* 12 (4) (1970) 268–277.
[17] S.F. Masri, T.K. Caughey, On the stability of the impact damper, *Journal of Applied Mechanics Transactions of the ASME* 33 (3) (1966) 586–592.
[18] M.M. Sadek, C.J.H. Williams, Effect of gravity on the performance of an impact damper: Part 2. Stability of vibrational modes, *Journal of Mechanical Engineering Science* 12 (4) (1970) 278–287.
[19] P.J. Holmes, The dynamics of repeated impacts with a sinusoidally vibrating table, *Journal of Sound and Vibration* 84 (2) (1982) 173–189.
[20] N. Popplewell, C.N. Bapat, K. McLachlan, Stable periodic vibroimpacts of an oscillator, *Journal of Sound and Vibration* 87 (1) (1983) 41–59.
[21] P.C. Pinotti, M.M. Sadek, Design procedure and charts for the impact damper, *Proceedings of the 11th International Machine Tool and Die Research Conference*, vol. A, 1970, pp. 181–195.
[22] S. Ema, E. Marui, A fundamental study on impact dampers, *International Journal of Machine Tools and Manufacture* 34 (3) (1994) 407–421.
[23] S.E. Semercigil, F. Collette, D. Huynh, Experiments with tuned absorber-impact damper combination, *Journal of Sound and Vibration* 256 (1) (2002) 179–188.
[24] A. Papalou, S.F. Masri, Performance of particle dampers under random excitation, *Journal of Vibration and Acoustics Transactions of the ASME* 118 (4) (1996) 614–621.
[25] I. Yokomichi, Y. Araki, Y. Jinnouchi, J. Inoue, Impact damper with granular material for multibody system, *Journal of Pressure Vessel Technology* 118 (1996) 95–103.
[26] C. Cempel, G. Lotz, Efficiency of vibrational energy dissipation by moving shot, *Journal of Structural Engineering* 119 (9) (1993) 2642–2652.
[27] A.Q. Liu, B. Wang, Y.S. Choo, K.S. Ong, The effective design of bean bag as a vibroimpact damper, *Shock and Vibration* 7 (6) (2000) 343–354.
[28] C. Pang, N. Popplewell, S.E. Semercigil, An overview of a bean bag damper's effectiveness, *Journal of Sound and Vibration* 133 (2) (1989) 359–363.
[29] N. Popplewell, S.E. Semercigil, Performance of the bean bag impact damper for a sinusoidal external force, *Journal of Sound and Vibration* 133 (2) (1989) 193–223.
[30] W. Goldsmith, *Impact: The Theory and Physical Behaviour of Colliding Solids*, Dover Publications, Mineola, New York, 1960.
[31] K.L. Johnson, *Contact Mechanics*, Cambridge University Press, Cambridge, 1985.
[32] M.S. Heiman, P.J. Sherman, A.K. Bajaj, On the dynamics and stability of an inclined impact pair, *Journal of Sound and Vibration* 114 (3) (1987) 535–547.